# $\beta$-decay half-lives of the $r$-process waiting-point isotones of $N = 81$ and 82 nuclei

C. Ma,[1] Y. Lu,[2] Y. Lei,[3] and Y. M. Zhao[1,4,*]

[1]*Shanghai Key Laboratory of Particle Physics and Cosmology, School of Physics and Astronomy, Shanghai Jiao Tong University, Shanghai 200240, China*
[2]*College of Physics and Engineering, Qufu Normal University, Qufu 273165, China*
[3]*School of National Defense Science and Technology, Southwest University of Science and Technology, Mianyang 621010, China*
[4]*Collaborative Innovation Center of IFSA (CICIFSA), Shanghai Jiao Tong University, Shanghai 200240, China*

(Received 17 November 2022; revised 18 February 2023; accepted 10 March 2023; published 27 March 2023)

In this paper we perform systematic calculations of $\beta$-decay half-lives for the $r$-process waiting-point isotones of $N = 81$ and 82, in the framework of nucleon-pair approximation. A phenomenological form of the Hamiltonian, which includes single-particle energies, pairing plus quadrupole interactions, and Gamow-Teller interactions is assumed, and the theoretical $\beta$-decay energies are taken based on the Bayesian machine learning. A good agreement with experimental values of half-lives is achieved by using the nucleon-pair truncated model space in which the $S$-pair condensation dominates. Our calculated half-lives are found to be very sensitive to $\beta$-decay energies on the one hand, and are quite robust with respect to extension of the model space and variation of interaction parameters on the other hand.

DOI: 10.1103/PhysRevC.107.034316

## I. INTRODUCTION

It has been well known that the rapid neutron-capture process (r-process) accounts for the nuclear synthesis of about half of elements heavier than iron [1–4]. Under very high temperatures ($T \approx 10^9$ K) and neutron densities ($>10^{20}$ cm$^{-3}$), the $r$-process mainly proceeds along the isotopic chains through successive neutron captures. The neutron capture rates are very sensitive to the neutron separation energies ($S_n$) [5,6]. A variation of 0.5 MeV in the separation energy would result in a change of a factor of approximately 2 to 5 in the neutron capture rates [5]. $S_n$ shows obvious discontinuities at the neutron magic numbers $N = 50$, 82, and 126, due to the shell closure. Consequently, rapid neutron capture reaction is greatly inhibited after arriving at these neutron magic numbers and has to wait for competing $\beta$ decays, bringing the nuclei into heavier isotopic chains. Thus reliable knowledge of $\beta$-decay half-lives at these waiting points are very important in the simulation of $r$-process networks [7].

Despite their importance in the $r$ process and great progresses in the experimental measurements [8–14], many half-lives of waiting point nuclei are not yet experimentally accessible, especially of those with $N = 126$. Those half-lives have to be evaluated by various theoretical methods, such as empirical methods [15,16], the quasiparticle random phase approximation (QRPA) [17–23], the nuclear shell model (NSM) [24–26], and the projected shell model (PSM) [27,28]. Among these approaches, the NSM is the most convincing theoretical method, because it appropriately takes two-body correlations among nucleons and thus push up the Gamow-Teller strength into relatively high excitation energies, consistent with experimental measurements. In Ref. [24], the half-lives and neutron-branching probabilities of the $N = 82$ waiting-point nuclei have been computed by the NSM considering the Gamow-Teller contribution. Those of the $N = 126$ isotones have also been studied by Suzuki in Ref. [25], and by Zhi in Ref. [26], in the framework of the NSM, which took into account both the Gamow-Teller (GT) and first-forbidden (FF) transitions. A systematic calculation of the $\beta$-decay half-lives for 5409 nuclei has been performed by Marketin and collaborators using the relativistic quasiparticle random phase approximation plus the relativistic Hartree-Bogoliubov model (RQRPA+RHB) in Ref. [23].

Although the NSM has been successfully applied into the $\beta$-decay simulations for those waiting-point nuclei, it suffers from the explosive dimension, which prohibits its application into more neutron-rich regions. Efficient and reliable truncation of the NSM is indispensable, and the nucleon-pair approximation (NPA) is one of popular truncation schemes, in which the configuration space is constructed by a few collective and noncollective nucleon pairs [29,30]. Because structure coefficients and spins of adopted nucleon pairs are variable, the NPA is very flexible in the numerical studies of nuclei in different mass regions and for different purposes, such as nuclear low-lying excitations [31–39], quantum phase transition [40,41], isoscalar pair correlation [42–44], and particle-hole excitations [45]. For a comprehensive review of the framework and recent applications of the NPA, one refers to Ref. [46].

The NPA approach has also been used to calculate the nuclear matrix elements of neutrinoless double-$\beta$ decay [47]. Yet, there has been no efforts to apply this useful method to the study of the conventional $\beta$ decays hitherto. The

*Corresponding author: ymzhao@sjtu.edu.cn

 

purpose of this paper is to report our systematic calculations of $\beta$-decay half-lives in the NPA framework. We focus on nuclei around the $N = 82$ waiting points, where experimental data are relatively rich to constrain our calculations and the FF contribution to the half-lives in this region is not significant in comparison with those in the $N = 126$ region. We are able to evaluate the half-lives of those very neutron-rich isotones, and discuss the robustness of our calculations with respect to larger configuration spaces, changes of interaction strength parameters, and $\beta$-decay energies. With simple assumption of $S$-pair condensation in the parent ground states, we find a good agreement of our calculated half-lives with experimentally accessible data of $N = 81$ and 82 isotones. The calculated half-lives are found to be very sensitive to the $\beta$-decay energies.

This paper is organized as follows. In Sec. II, we will briefly introduce the Fermi $\beta$-decay theory and the NPA formulation, including the formulation of half-life evaluation, Hamiltonian, and the NPA configuration space. The inputs of our parameters and calculated results together with discussions of robustness of our calculations, are presented in Sec. III. Finally our summary and perspectives are given in Sec. IV.

## II. FRAMEWORK OF OUR CALCULATIONS

Let us begin our discussion with a brief introduction to Fermi theory of $\beta$ decay [48]. For most $\beta$-decay processes, the kinetic energies of electrons and neutrinos are in the order of 1 MeV, corresponding to wave lengths $\lambda \approx 10^2$ fm which is much larger than the nuclear size, as a consequence, the allowed transitions are the most important parts of the processes. The GT decay rate from the $j$th state of the parent nucleus to the $i$th state of the corresponding daughter nucleus is given by

$$\lambda_{ij}^{\mathrm{GT}} = CB_{ij}^{\mathrm{GT}} f(Z_D, A, Q_\beta + E_j - E_i) , \tag{1}$$

where $C = 0.11246\ \mathrm{ms}^{-1}$, and $E_i$, $E_j$ are the excitation energy of corresponding states. The $\beta$-decay energy $Q_\beta = m_P - m_D - m_e$, where $m_P$, $m_D$, and $m_e$ are the inertia masses of parent nucleus, daughter nucleus, and electron from either experimental measurements or theoretical estimations; $B_{ij}^{\mathrm{GT}}$ is the GT transition strength from the $j$th state of the parent nucleus to the $i$th state of the daughter nucleus,

$$B_{ij}^{\mathrm{GT}} = \frac{2I_{D_i} + 1}{2I_{P_j} + 1} g_A^2 |\langle D_i || \sigma\tau_\pm || P_j \rangle|^2 , \tag{2}$$

where $I_{D_i}$ and $I_{P_j}$ are the angular momenta of the final state and the initial state, respectively, $g_A$ is the effective axial coupling constant, $\langle D_i || \sigma\tau_\pm || P_j \rangle$ is the reduced GT matrix element, $\sigma$ is the Pauli spin operator, and $\tau_\pm$ is the isospin ladder operator. Technical details related to this reduced matrix element in the NPA framework is presented in the Appendix. The $f(Z_D, A, Q_\beta + E_j - E_i)$ in Eq. (1) is the energy integral accounting for the contribution of lepton phases, and has a dependence on the proton number of the daughter nucleus, $Z_D$, the mass number $A$, and the transition energy $(Q_\beta + E_j - E_i)$, and is written as

$$f(Z, A, E) = \int_1^{\omega_0} F(Z, A, \omega)\sqrt{\omega^2 - 1}(\omega_0 - \omega)^2 \omega d\omega, \tag{3}$$

where $\omega_0 = E/m_e c^2$ is the maximum electron energy in units of electron mass. The $F(Z, A, \omega)$ is the Fermi function, which takes into account the distortion of electron wave function from the nuclear Coulomb field [49], and we take the analytical form of $F(Z, A, \omega)$ from Ref. [50] in this paper. The $\beta$-decay half-life of the $j$th parent state is directly related to the decay rates by

$$T_{1/2}^j = \frac{\ln 2}{\sum_i \lambda_{ij}^{\mathrm{GT}}} . \tag{4}$$

Now we come to the shell model Hamiltonian $H$ of this paper. $H$ here includes the single-particle term, pairing plus quadrupole interaction, and the Gamow-Teller force,

$$H = H_0 + H_P + H_{QQ} + H_{\mathrm{GT}} . \tag{5}$$

$H_0$ represents the conventional spherical single-particle energy term, for which the single-particle energies are fixed either from the experimental spectrum of nuclei with only one valence nucleon or from systematic studies. The second term on the right hand side of Eq. (5),

$$H_P = \sum_\eta -G_\eta \mathcal{P}_\eta^\dagger \mathcal{P}_\eta - G_\eta^{(2)} \mathcal{P}_\eta^{(2)\dagger} \cdot \mathcal{P}_\eta^{(2)} , \tag{6}$$

represents the residual two-body monopole plus quadrupole pairing interaction between the valence protons ($\eta = \pi$) or the valence neutrons ($\eta = \nu$). The third term,

$$H_{QQ} = -\sum_\eta \kappa_\eta : Q_\eta \cdot Q_\eta : -\kappa Q_\pi \cdot Q_\nu , \tag{7}$$

is the residual quadrupole-quadrupole interaction between valence protons, valence neutrons, and valence protons and valence neutrons. The symbol :: means the normal order product of nucleon operators involved in the quadrupole-quadrupole interaction. The quadrupole pairing and quadrupole-quadrupole interactions between like-valence particles play opposite roles in the nuclear deformation, and this provides a foundation of the phenomenological shell model Hamiltonian in describing the low-lying structures for both spherical and deformed even-even nuclei [51]. The monopole pairing strength $G_\eta$, is adopted to be about $27/A$ MeV, and the quadruple pairing strength, $G_\eta^{(2)}$, is taken to be about one order of magnitude smaller than $G_\eta$ [31]. We also take the empirical value of the proton-neutron quadrupole-quadrupole interaction strength, summarized in Ref. [31], $\kappa = 186/A^{5/3}$, and the strengths between like nucleons, $\kappa_\eta$, are close to the half of $\kappa$. The last term in Eq. (5) is the so-called Gamow-Teller force,

$$H_{\mathrm{GT}} = 2\chi_{\mathrm{GT}} \sum_\mu : \beta_\mu^{(1)} \beta_\mu^{(1)\dagger} : -2\kappa_{\mathrm{GT}} \sum_\mu \Gamma_\mu^{(1)} \Gamma_\mu^{(1)\dagger} . \tag{8}$$

It is a charge-dependent neutron-proton interaction with both particle-hole (p-h) and particle-particle (p-p) channels. Such a phenomenological interaction was used to study the nuclear single- and double-$\beta$ decay within the frameworks of the

QRPA [52–55] and the PSM [27,28]. There have been two sets of parameters for $H_{\rm GT}$; one optimized in Ref. [52], with $\chi_{\rm GT} = 23/A$ and $\kappa_{\rm GT} = 7.5/A$, and another set, optimized in Ref. [53], with $\chi_{\rm GT} = 5.2/A^{0.7}$ and $\kappa_{\rm GT} = 0.58/A^{0.7}$. In this paper we have taken the latter set of parameters for $H_{\rm GT}$.

The spherical tensor operators in Eqs. (6)–(8) are defined as follows:

$$\begin{aligned}
\mathcal{P}_\eta^\dagger &= \sum_{j_\eta} \frac{\sqrt{2j_\eta+1}}{2}\left(a_{j_\eta}^\dagger \times a_{j_\eta}^\dagger\right)^{(0)}, \\
\mathcal{P}_\eta^{(2)\dagger} &= \sum_{j_\eta j'_\eta} q_2(j_\eta j'_\eta)\left(a_{j_\eta}^\dagger \times a_{j'_\eta}^\dagger\right)^{(2)}, \\
Q_\eta &= \sum_{j_\eta j'_\eta} q_2(j_\eta j'_\eta)\left(a_{j_\eta}^\dagger \times \tilde{a}_{j'_\eta}\right)^{(2)}, \\
\beta^{(1)} &= \sum_{j_\pi j_\nu} q_1(j_\pi j_\nu)\left(a_{j_\pi}^\dagger \times \tilde{a}_{j_\nu}\right)^{(1)}, \\
\Gamma^{(1)} &= \sum_{j_\pi j_\nu} q_1(j_\pi j_\nu)\left(a_{j_\pi}^\dagger \times a_{j_\nu}^\dagger\right)^{(1)},
\end{aligned} \tag{9}$$

where $a_{jm}^\dagger$ is the single-particle creation operator and we taken the convention $\tilde{a}_{jm} = (-)^{j-m}a_{j-m}$ for time-reversal annihilation operators. The structure coefficient $q_1(j_\pi j_\nu)$ is taken as

$$\begin{aligned}
q_1(j_\pi j_\nu) &= \delta_{n_\pi n_\nu}\delta_{l_\pi l_\nu}\sqrt{2(2j_\pi+1)(2j_\nu+1)} \\
&\quad \times (-)^{l_\pi+j_\pi+\frac{3}{2}}\begin{Bmatrix} \frac{1}{2} & \frac{1}{2} & 1 \\ j_\nu & j_\pi & l_\pi \end{Bmatrix},
\end{aligned} \tag{10}$$

while $q_2(j_\eta j'_\eta)$ has the form

$$\begin{aligned}
q_2(j_\eta j'_\eta) &= \frac{(-)^{j_\eta+\frac{1}{2}}}{\sqrt{20\pi}}\sqrt{(2j_\eta+1)(2j'_\eta+1)} \\
&\quad \times C^{20}_{j_\eta 1/2,\, j'_\eta-1/2}\langle n_\eta l_\eta|r^2|n'_\eta l'_\eta\rangle .
\end{aligned} \tag{11}$$

Here, $\delta$ is the Kronecker delta symbol, $n_\eta$ ($n'_\eta$) and $l_\eta$ ($l'_\eta$) are the radial and orbital quantum numbers, and $\{ \vdots \}$ denotes a $6j$ symbol. $C^{j_3 m_3}_{j_1 m_1, j_2 m_2}$ is the Clebsch-Gordan coefficient, and the matrix elements of $r^2$ are given in Ref. [56]. We note that $\beta^{(1)}$ is the second-quantized form of $\sigma\tau_-$, and $Q_\eta$ is the second-quantized form of $r^2 Y^{(2)}$ between like nucleons ($\eta = \pi$ or $\nu$).

The NPA adopts collective nucleon-pair basis states, instead of single-particle Slater determinants, as building blocks of the configuration space. A collective pair of like valence nucleons with spin number $r$ is defined as

$$A_\eta^{(r)\dagger} = \sum_{j_\eta j'_\eta} y(j_\eta j'_\eta r)\left(a_{j_\eta}^\dagger \times a_{j'_\eta}^\dagger\right)^{(r)}, \tag{12}$$

where $y(j_\eta j'_\eta r)$ is called the structure coefficient of the nucleon pair. For an even-even (e-e) nucleus with $2N_\pi$ valence protons and $2N_\nu$ valence neutrons, the basis of the NPA configuration space is given by stepwise coupling $N_\pi$ proton pairs and $N_\nu$ neutron pairs. For an odd-mass (o-e or e-o) or odd-odd (o-o) nucleus, additional single-particle creation operator(s) is (are) coupled to the basis states of the corresponding even-even core. If one considers all possible nucleon pairs, the nucleon-pair basis is equivalent to that of the NSM. In many cases, the low-lying structures of medium and heavy mass nuclei can be well described in the space constructed by $S$ ($r = 0$) and $D$ ($r = 2$) pairs, as shown in previous studies, e.g., [31–34,36].

In this work, we mainly focus on the $\beta$-decay of parent ground states for isotones with $N = 81$ and 82. These nuclei are close to spherical, and thus the $S$-pair condensation picture of valence protons is expected to be reliable in ground states. Our model spaces of parent nuclei under the nucleon-hole representation are given by

$$\begin{aligned}
&\left(A_\pi^{(0)\dagger}\right)^{N_\pi}|0\rangle \text{ for e-e nuclei,} \\
&a_{j_\pi}^\dagger\left(A_\pi^{(0)\dagger}\right)^{N_\pi}|0\rangle \text{ for o-e nuclei,} \\
&\left(A_\pi^{(0)\dagger}\right)^{N_\pi}a_{j_\nu}^\dagger|0\rangle \text{ for e-o nuclei,} \\
&\left(a_{j_\pi}^\dagger\left(A_\pi^{(0)\dagger}\right)^{N_\pi} \times a_{j_\nu}^\dagger\right)^{I_P}|0\rangle \text{ for o-o nuclei}
\end{aligned} \tag{13}$$

with $j_\pi$, $j_\nu$, and $I_P$ running over all proton and neutron single-particle levels, and all possible coupled angular momentum, respectively. The dimension of our model space for parent nuclei is extremely small: one in the e-e case, a very few in the odd mass case, and a few dozens in the o-o case. Such assumption would be reduced to the generalized seniority scheme if the structure coefficients were so specifically chosen that follow Eqs. (23.5) and (23.7) of Ref. [57]. In this paper, our structure coefficients of nucleon pairs are optimized by minimizing the ground state energy of the NPA calculation for individual nucleus, resorting to the Levenberg-Marquardt algorithm [58,59]. This algorithm interpolates between the Gauss-Newton algorithm and the method of gradient descent, and achieve much more robustness and efficiency in the nonlinear least squares problems.

As for daughter nuclei, states connected with parent configurations by the GT operator could populate several MeV above the ground states, where conventional $SD$-pair truncation scheme is not good. On the other hand, fortunately, the GT operator is a single-particle operator which breaks at most one collective pair in the parent nucleus; therefore one non-collective pair coupled to $S$ pair condensate ground state of the parent nucleus suffices the configuration space of the GT transition calculations. Our model spaces of daughter nuclei with the nucleon-hole representation are

$$\begin{aligned}
&\left(a_{j'_\pi}^\dagger\left(A_\pi^{(0)\dagger}\right)^{N_\pi\text{-}1} \times a_{j'_\nu}^\dagger\right)^{I_D}|0\rangle , \\
&\left(\left(a_{j_\pi}^\dagger \times a_{j'_\pi}^\dagger\right)^{(J_\pi)}\left(A_\pi^{(0)\dagger}\right)^{N_\pi\text{-}1} \times a_{j'_\nu}^\dagger\right)^{I_D}|0\rangle , \\
&\left(a_{j'_\pi}^\dagger\left(A_\pi^{(0)\dagger}\right)^{N_\pi\text{-}1} \times \left(a_{j_\nu}^\dagger \times a_{j'_\nu}^\dagger\right)^{(J_\nu)}\right)^{I_D}|0\rangle , \\
&\left(\left(a_{j_\pi}^\dagger \times a_{j'_\pi}^\dagger\right)^{(J_\pi)}\left(A_\pi^{(0)\dagger}\right)^{N_\pi\text{-}1} \times \left(a_{j_\nu}^\dagger \times a_{j'_\nu}^\dagger\right)^{(J_\nu)}\right)^{I_D}|0\rangle ,
\end{aligned} \tag{14}$$

for o-o, e-o, o-e, and e-e daughter nuclei, respectively. Here, $a_{j_\pi}^\dagger$, $a_{j'_\pi}^\dagger$, $a_{j_\nu}^\dagger$, and $a_{j'_\nu}^\dagger$ represent the single-particle creators, and $J_\pi$, $J_\nu$, $I_D$ denote the coupled angular momenta. In this paper, we take *all* possible, noncollective, broken pairs into consideration, although not all of them are necessary in the calculation of $\beta$-decay half-lives.

TABLE I. Parameters of the Hamiltonian (in MeV) in this work. The single-particle energies are taken the experimental data of Ref. [60] except that the energies of the $0h_{11/2}$, $1p_{1/2}$, and $1p_{3/2}$ orbits are taken from Refs. [61–63]. The parameters of residual interactions are optimized to fit experimental spectra of $^{130}$Cd, $^{130}$Sn, and $^{130}$In, respectively.

| | | | | | |
|---|---|---|---|---|---|
| $j_\pi$ | $1p_{1/2}$ | $1p_{3/2}$ | $0f_{5/2}$ | $0g_{9/2}$ | |
| $\epsilon_{j_\pi}$ | 0.365 | 1.353 | 2.750 | 0.000 | |
| $j_\nu$ | $2s_{1/2}$ | $1d_{3/2}$ | $1d_{5/2}$ | $0g_{7/2}$ | $0h_{11/2}$ |
| $\epsilon_{j_\nu}$ | 0.332 | 0.000 | 1.655 | 2.434 | 0.065 |

| | | |
|---|---|---|
| $G_\pi$ | $G_\pi^{(2)}$ | $\kappa_\pi$ |
| $29/A$ | $2.9/A$ | $150/A^{5/3}$ |
| $G_\nu$ | $G_\nu^{(2)}$ | $\kappa_\nu$ |
| $20/A$ | $2.0/A$ | $150/A^{5/3}$ |
| $\chi_{\rm GT}$ | $\kappa_{\rm GT}$ | $\kappa$ |
| $5.2/A^{0.7}$ | $0.58/A^{0.7}$ | $200/A^{5/3}$ |

## III. RESULTS AND DISCUSSION

In this section we discuss our parametrizations, calculated results as well as the robustness of our predictions.

### A. Parameters

In this work we apply the NPA to the $\beta$-decay half-lives of isotones with neutron number $N = 81$ and 82 and the proton number $38 \leqslant Z \leqslant 49$. A computer code has been developed for this purpose under the basis states of Ref. [30]. The input of our code includes the single-particle levels and corresponding energies, the parameters of the Hamiltonian, the $\beta$-decay energies, and the effective axial coupling constant.

We adopt the $pf$ shell for valence protons and the $sdg$ shell for valence neutrons, namely, valence proton holes in the $1p_{1/2}$, $1p_{3/2}$, $0f_{5/2}$, and $0g_{9/2}$ levels, and valence neutron holes in $2s_{1/2}$, $1d_{3/2}$, $1d_{5/2}$, $0g_{7/2}$, and $0h_{11/2}$ levels. Without confusion, we use $\frac{1}{2}^-, \frac{3}{2}^-, \frac{5}{2}^-, \frac{9}{2}^+$, and $\frac{1}{2}^+, \frac{3}{2}^+, \frac{5}{2}^+, \frac{7}{2}^+, \frac{11}{2}^-$, to denote those single-particle levels for short. In Table I, we present the single-particle energies based on experimental spectra of Ref. [60], except that we take the results of $\frac{11}{2}^-$ from Ref. [61], of $\frac{1}{2}^-$ from Ref. [62], and of $\frac{3}{2}^-$ from Ref. [63], respectively.

There are in total nine parameters for two-body residual interactions in the Hamiltonian of Eq. (5), $G_\pi$, $G_\pi^{(2)}$, $\kappa_\pi$ for proton-proton part, $G_\nu$, $G_\nu^{(2)}$, $\kappa_\nu$ for neutron-neutron part, and $\chi_{\rm GT}$, $\kappa_{\rm GT}$, $\kappa$ for neutron-proton part. In this work, these strength parameters are assumed to follow the mass number dependence compiled in Appendix B of Ref. [31], and they are readjusted to achieve the best fit of experimental spectra, by using $^{130}$Cd for proton-proton part, by using $^{130}$Sn for neutron-neutron part, and by using $^{130}$In for proton-neutron part. The optimized parameters are shown in Table I. Here, we assume a slightly larger value for the monopole pairing strength of protons in comparison with that of neutrons, as in earlier calculations [31–33]. The quadrupole pairing strengths are an order of magnitude smaller than corresponding $G_\eta$. For the quadrupole-quadrupole terms, the strengths for like nucleons $\kappa_\eta$ are slightly larger than half of the neutron-proton strength. $\chi_{\rm GT}$ and $\kappa_{\rm GT}$ follow the systematic formulas of Ref. [53]. The robustness of our calculation to these parameters will be discussed in Sec. III C.

In Fig. 1, we present calculated spectra of those three nuclei, $^{130}$Sn, $^{130}$Cd, and $^{130}$In, which are used to fix our parameters of our Hamiltonian. One sees a good agreement between the calculated results and experimental data excited up to about 4 MeV [64], except that the $8^+$ state in $^{130}$Cd, the $10^+$ state in $^{130}$Sn, and the $3^+$ and $5^+$ states in $^{130}$In are a few hundreds of keV lower than experimental data. The dominant components in these states have been well known, namely, $(a^\dagger_{9/2^+} \times a^\dagger_{9/2^+})^{(8)}$ for the $8_1^+$ state of $^{130}$Cd, $(a^\dagger_{11/2^-} \times a^\dagger_{11/2^-})^{(10)}$ for the $10_1^+$ state of $^{130}$Sn, and $(a^\dagger_{9/2^+} \times a^\dagger_{3/2^+})^{(3,5)}$ for the lowest $3^+$ and $5^+$ states of $^{130}$In, respectively. We note that one is able to further improve the agreement between calculated results and experimental data for these isotones by considering higher order pairing interactions as in Ref. [37], or by introducing monopole correction terms as in Refs. [65–69]. However, such additional interaction terms does not improve calculated $\beta$-decay half-lives, and therefore we do not consider those interaction terms, for simplicity. On the other hand, the Gamow-Teller interaction is indispensable here, because the calculated $1^+$ state energy in $^{130}$In, an important daughter state of the GT transition from $^{130}$Cd, is very sensitive to this interaction.

The $\beta$-decay energy is another parameter in our calculations. Unfortunately, for most isotones considered in this paper, the $\beta$-decay energy is not accessible in the latest atomic mass evaluation, the AME2020 database [70], except those for $^{129}$Cd, $^{130}$Cd, $^{130}$In, and $^{131}$In. Therefore one has to resort to theoretical mass evaluations, to extract $\beta$-decay energies, defined by

$$Q_\beta(N,Z) = M(N,Z) - M(N-1, Z+1)\,, \qquad (15)$$

where $M(N,Z)$ is atomic mass of nucleus with $N$ neutrons and $Z$ protons. Very recently, a nuclear-mass prediction within accuracy required by $r$-process studies (abbreviated as "BML" in this paper) [71] was proposed by using the Bayesian neural networks, and we adopt this set of predicted database as one of our mass inputs. As comparison, we also extract the $Q_\beta$ from other theoretical mass models, such as the finite-range droplet mass model (denoted by "FRDM") [72], the systematics of neutron-proton interactions (denoted by "VNP") [73], and the Weizsäcker-Skyrme mass model (denoted by "WS4") [74]; the FRDM and WS4 models are global macroscopic-microscopic mass models, and the VNP results are based on local mass formulas involving of neighboring nuclei. In experimental accessible region of $A \approx 130$, the accuracies of these four models are close to 0.1 (BML), 0.5 (FRDM), 0.2 (VNP) and 0.3 (WS4) MeV.

In Fig. 2 we plot the $\beta$-decay energies from these model for $N = 81$ and 82 isotones, together with the experimental values (EXP) and those predicted in the AME2020 database (PRE). $Q_\beta$ exhibit distinct odd-even staggering with magnitudes 2–4 MeV originating from the pairing correlation. From the figure, One sees the BML results not only consist with accessible experimental data, but also includes a "safe" error

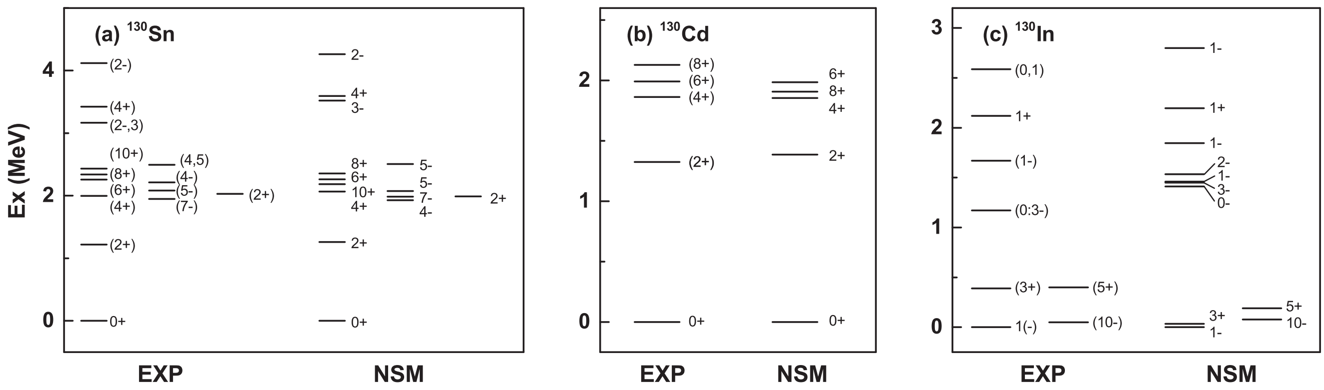


FIG. 1. Energy levels of three nuclei, (a) $^{130}$Sn, (b) $^{130}$Cd, and (c) $^{130}$In, which are used to fix parameters in our calculations. Experimental data (denoted by "EXP") are taken from Ref. [64]. The results denote by "NSM" are the nuclear shell-model results calculated by using the parameters in Table I.

bar which covers all other three sets of the theoretical values (although the confidence intervals grow rapidly from 0.4 to 4.6 MeV for $N = 82$ isotones, and from 0.4 to 3.9 MeV for $N = 81$ isotones). Therefore we adopt predicted results of the BML model in our calculation.

Now let us look at the parametrization of the effective axial strength $g_A$. For the $\beta$ decay of $N = 82$ isotones, we fix $g_A$ by reproducing the half-life from the ground $9/2^+$ state of $^{131}$In to the excited $7/2^+$ state of $^{131}$Sn. In our model space, the GT operator is as follows:

$$\sigma_\mu \tau_- = q_1(9/2^+ 7/2^+)(a^\dagger_{9/2^+} \times \tilde{a}_{7/2^+})^{(1)}_\mu$$
$$= \sqrt{\frac{160}{27}}(a^\dagger_{9/2^+} \times \tilde{a}_{7/2^+})^{(1)}_\mu . \quad (16)$$

Considering the fact that the configuration of $^{131}$In ground state is a $\frac{9}{2}^+$ proton hole and that of $^{131}$Sn excited state is a $\frac{7}{2}^+$ neutron hole, we arrive at

$$\log(ft) = \log(\ln 2/CB^{\mathrm{GT}}) = 3.54 - 2\log(g_A)\,, \quad (17)$$

for which the experimental result is $\log(ft) = 4.4$ [64], and our resultant $g_A = 0.40$ for the $N = 82$ isotones. Similarly, we obtain $g_A = 0.47$ for $N = 81$ isotones by using the half-life from the ground $(a^\dagger_{9/2^+} \times a^\dagger_{11/2^-})^{(1)}$ state of $^{130}$In to the $(a^\dagger_{11/2^-} \times a^\dagger_{7/2^+})^{(2)}$ state of $^{130}$Sn, for which the experimental value $\log(ft) = 4.2$ [64]. It is worthy to note that our effective $g_A$ values (0.40 for the $N = 82$ isotones and 0.47 the $N = 81$ isotones) are relatively smaller than those adopted in the $\beta$ decay studies of nuclei with $A \approx 130$ by using the shell model calculations, in which the effective $g_A$ values are from 0.52 to 0.94 (see Table 1 of Ref. [75]), because the nucleon-pair truncation further intensifies the quenching effect of $g_A$.

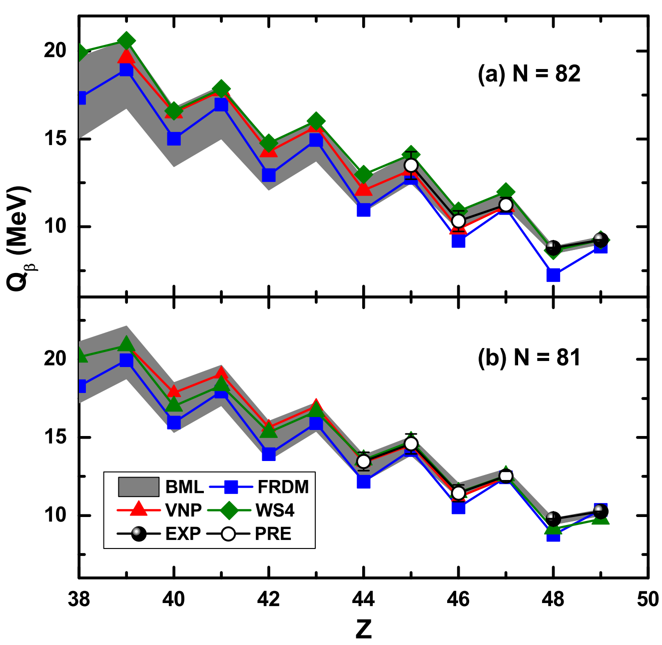


FIG. 2. $Q_\beta$ values for $N = 81$ and 82 isotones versus proton number $Z$. Experimental data and those predicted in the AME2020 database [70] are plotted by using black balls in solid and hollow black balls. The theoretical values extracted from the FRDM [72], the systematics of proton-neutron interactions [73] and the WS4 model [74] are presented by using blue squares, red triangles, and green diamonds, respectively. The regions in dark grey are plotted by using the confidence intervals of $Q_\beta$ predicted by the Bayesian machine learning (BML) mass model [71].

### B. Calculated results

In this subsection, we discuss our calculated results by using parameters obtained above. In Fig. 3, we plot the energy spectra for even-odd, odd-even and odd-odd parent nuclei, the model space of which includes a number of excited states. In the first two panels, the results of states with different spins are presented in different colors, while in the last panel for odd-odd nuclei, we plot the states of different configurations (i.e., unpaired proton hole and unpaired neutron hole) by using different colors. From this figure, one clearly sees how excited state energies of isotones evolve as going to the more neutron-rich regions (i.e., nuclei with less proton number).

With our pairing plus quadrupole interaction between valence proton-holes, for the $N = 82$ isotones with odd proton numbers, the energies of the $\frac{1}{2}^-$, $\frac{3}{2}^-$, and $\frac{5}{2}^-$ states gradually decreases with respect to the $\frac{9}{2}^+$ state, while the gap between

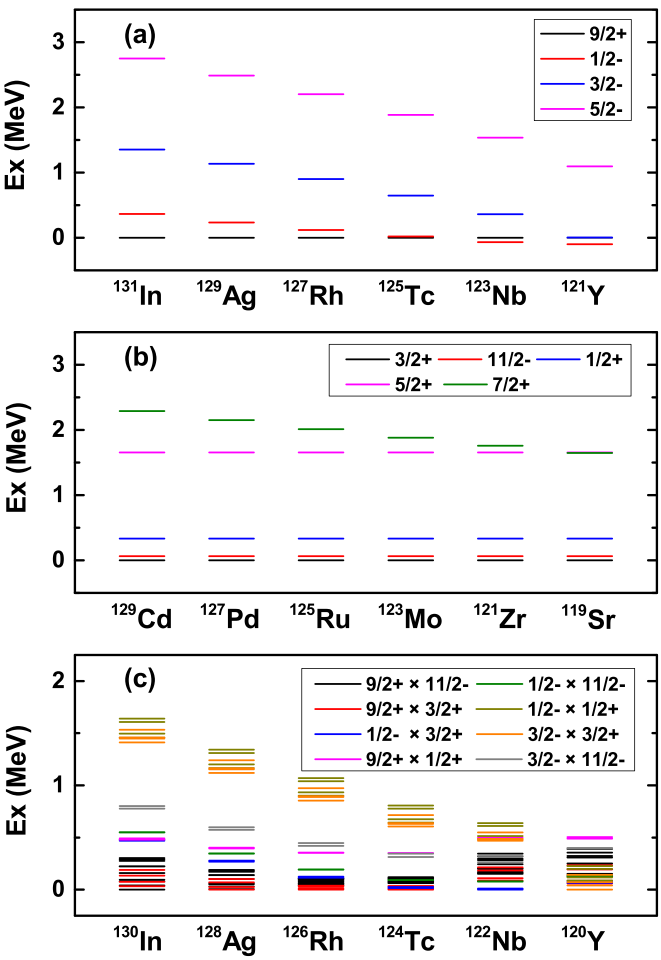


FIG. 3. Calculated energy spectra of parent nuclei. (a) corresponds to $N = 82$ isotones with odd numbers of protons; (b) corresponds to $N = 81$ isotones with even numbers of protons, and (c) corresponds to $N = 81$ isotones with odd numbers of protons. In (c) we use different colors for configurations of different orbits in which the unpaired nucleons fill. See text for detailed description.

$\frac{3}{2}^-$ and $\frac{5}{2}^-$ states remains almost unchanged. The $\frac{1}{2}^-$ state is nearly degenerate with the $\frac{9}{2}^+$ state for $^{125}$Tc and crosses over for $^{123}$Nb. As for the $N = 81$ isotones with even proton numbers, the states involved in this paper are essentially given by the single-particle excitations of the unpaired neutron hole, the valence proton holes are $S$-pair condensation and serve as a "spectator". As a consequence, the monopole pairing, quadrupole pairing and quadrupole-quadrupole interactions between valence like-nucleon holes does not change in the small configuration space adopted here for given nucleus, and the neutron-proton quadrupole interaction vanishes because $\langle S^{N_\pi}||Q_\pi||S^{N_\pi}\rangle = 0$. The only active term in the Hamiltonian is the GT interaction, which has attractive property due to the monopole contribution [76], namely,

$$\overline{H}_{\rm GT}(j_\pi, j_\nu) = \frac{\sum_J (2J+1)\langle j_\pi j_\nu | H_{\rm GT} | j_\pi j_\nu\rangle_J}{\sum_J (2J+1)} < 0 ,$$

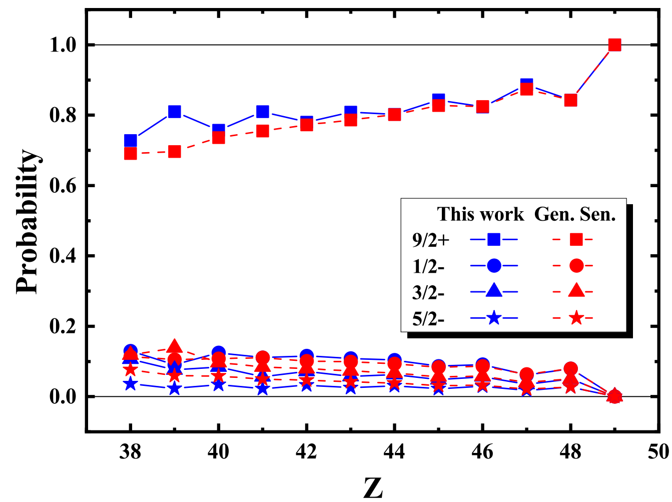


FIG. 4. Occupation probability of the proton orbits in the ground states of $N = 82$ isotones by our optimized $S$-pair truncation. Results of the generalized seniority scheme are plotted for comparison.

where $j_\pi$ represents the proton-hole $g^+_{9/2}$ orbit, and $j_\nu$ represents the neutron-hole $g^+_{7/2}$ orbit. The attractive $\overline{H}_{\rm GT}(j_\pi, j_\nu)$ leads to a decrease of the neutron $g^+_{\frac{7}{2}}$ orbit with the pair number of proton holes (i.e., nuclei with less protons), as shown in Fig. 3(b). For odd-odd nuclei involved in this paper, as usual, the low-lying energy spectra are much more complicated, because in this case all terms in the Hamiltonian, the pairing plus quadrupole interaction, the GT interaction and the monopole correction play essential roles. Yet one sees similar patterns exhibited in panel (a)—the states with $\frac{1}{2}^-$, $\frac{3}{2}^-$ unpaired proton gradually decreases with pair number of proton holes, and cross over states involving of the $\frac{9}{2}^+$ configuration for $^{122}$Nb.

As we have mentioned in last section, the structure coefficients of the proton $S$ pairs are obtained by minimizing the ground state energies of parent nuclei. Here, a natural question is whether or not there is sizable difference between calculated results by using such optimized nucleon pairs and those within the framework of the simple and well-known generalized seniority scheme. To answer this question, we have also performed a generalized seniority calculation, with the $S$-pair structure coefficients of valence proton holes fixed by using the optimized result of $^{130}$Cd. In Fig. 4, we present the probability of proton holes occupying different proton orbits for these two sets of the ground states of the $N = 82$ isotones. One sees that both calculations present about 80% of the proton holes in the $\frac{9}{2}^+$ level, while those in the $\frac{1}{2}^-$, $\frac{3}{2}^-$, and $\frac{5}{2}^-$ levels are around 10%. Both sets of the probabilities gradually evolve with pair number of proton holes in a similar manner. On the other hand, one also sees that the two states are very close to each other for $^{130}$Cd, $^{128}$Pd, and $^{126}$Ru, while sizable differences arise for proton-rich nuclei with odd protons. As a consequence, those isotones with odd protons decay faster for our optimized-$S$ approximation than for the generalized seniority scheme.

Our calculated half lives for the ground states of $N = 81$ and 82 isotones with proton numbers $Z = 39$-49 are shown in

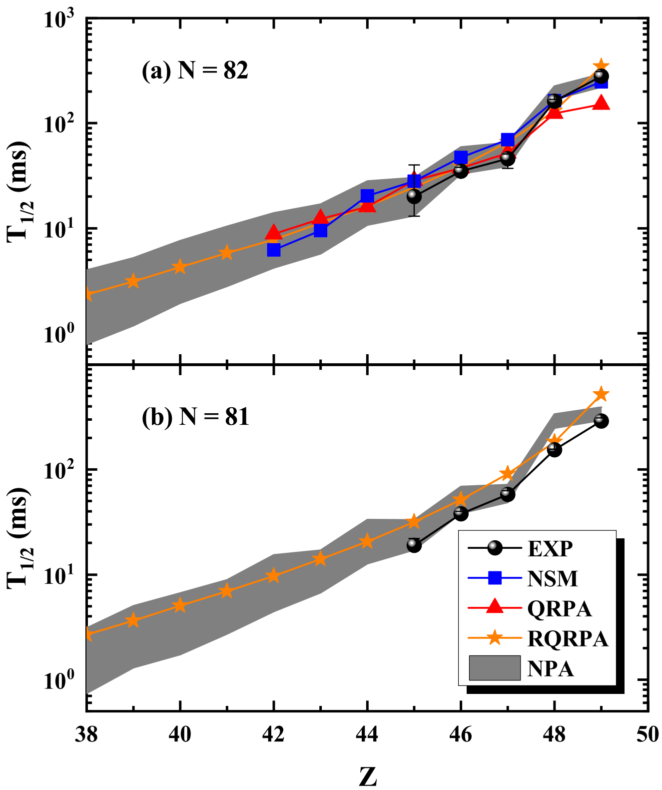


FIG. 5. $\beta$-decay half-lives for $N = 82$ and 81 isotones versus proton number $Z$. (a) corresponds to $N = 82$, and (b) corresponds to $N = 81$. Experimental data, and theoretical results from the NSM [26], the QRPA + HFB21 [21], and the RQRPA + RHB [23] methods, are also presented in black, blue, red, and orange, respectively. The range in dark grey represents our predicted half-lives with uncertainties originated from the nuclear masses.

Fig. 5, and are compared to the accessible experimental data. We also plot in the figure the results of some other models as comparisons: the NSM [26], the QRPA + HFB21 [21], and the RQRPA + RHB [23] for the $N = 82$ isotones, and the RQRPA + RHB [23] for the $N = 81$ isotones. In Table II we list calculated half-lives and corresponding theoretical uncertainties originated from the mass errors predicted in the BML mass model. Compared to other theoretical results, our calculations well reproduce the half-lives of $^{131}$In, $^{130}$Cd, $^{129}$Ag, and $^{128}$Pd, and especially the sudden decreases from $^{130}$Cd to $^{129}$Ag, which was underestimated in the three sets of previous calculations. For more neutron-rich isotones, one sees that the $\beta$-decay half-lives of the $N = 82$ isotones predicted in this work are well consistent with the previous results in Refs. [21,23,26]. For the $N = 81$ isotones, the RQRPA+RHB method predicts the $\beta$-decay half-lives a little bit longer than the experimental data. Our results agree better with the experimental data, except for a slightly longer half-life for $^{129}$Cd.

Figure 6 shows the partial decay rates $\lambda_{ij}^{\mathrm{GT}}$ which correspond to the dominant GT contribution to $\beta$-decay half-lives, as a function of excitation energy of final state of the daughter nucleus. From the figure, one sees that the decay rates from most odd-even, even-odd, and odd-odd nuclei are densely fragmented by many excited states, while those from the even-even nuclei [Fig. 6(b), 6(d), 6(f), 6(h), 6(j), 6(l)] are contributed by only one excited state. This is because only one $1^+$ state can be constructed in the model space of daughter odd-odd nuclei, namely,

$$\left(a^{\dagger}_{\frac{9}{2}^+}\left(A_{\pi}^{0\dagger}\right)^{N_{\pi}} \times a^{\dagger}_{\frac{7}{2}^+}\right)^{(1)}|0\rangle \; .$$

In Fig. 6(i) and 6(k), one sees that the fragmentation for $^{123}_{41}\mathrm{Nb}_{82}$ and $^{121}_{39}\mathrm{Y}_{82}$ decays is sparse. This is easy to understand—both ground state spins of these two parent nuclei are $\frac{1}{2}^-$, thus there are only two spins, $\frac{1}{2}^-$ and $\frac{3}{2}^-$, of daughter nuclei, connected to the ground state spins of parent nuclei by the GT operator, and furthermore, there are only two cases of noncollective proton-hole pair $(a^{\dagger}_{1/2^-}a^{\dagger}_{9/2^+})^{(J)}$, i.e., $J = 4$ or 5, in the daughter nucleus.

One also sees from Fig. 6 that the excited energy of daughter nuclei for GT-transition peaks increases with pair number of valence proton holes, gradually from 2 to 8 MeV. For $^{128}$Pd, $^{126}$Ru, and $^{124}$Mo, the energies of the GT transition peaks are about 2.5–3.0 MeV above the daughter ground states, which are slightly higher than the results calculated by the NSM (see Fig. 11 in Ref. [26]). One also sees that the energies for peaks of odd-$Z$ parent nuclei are higher than those of their

TABLE II. Calculated $\beta$-decay half-lives and their uncertainties (in ms) (related to the uncertainties of theoretical mass predicted in the BML model [71]) for the $N = 82$ and 81 isotones. Experimental data and theoretical results of the NSM [26], the QRPA+HFB21 [21], and the RQRPA+RHB method [23] are also tabulated for comparison.

| Nucl. | $^{131}$In | $^{130}$Cd | $^{129}$Ag | $^{128}$Pd | $^{127}$Rh | $^{126}$Ru | $^{125}$Tc | $^{124}$Mo | $^{123}$Nb | $^{122}$Zr | $^{121}$Y | $^{120}$Sr |
|---|---|---|---|---|---|---|---|---|---|---|---|---|
| Exp. | $280 \pm 30$ | $162 \pm 7$ | $46^{+5}_{-7}$ | $35 \pm 3$ | $20^{+20}_{-7}$ | | | | | | | |
| NSM | 248 | 164 | 69.8 | 47.3 | 28.0 | 20.3 | 9.52 | 6.21 | | | | |
| QRPA | 151 | 124 | 51.8 | 37.4 | 28.4 | 16.0 | 12.3 | 8.82 | | | | |
| RQRPA | 346 | 131 | 65.8 | 38.8 | 24.4 | 16.2 | 11.2 | 7.78 | 5.79 | 4.27 | 3.12 | 2.34 |
| NPA | $255^{+39}_{-33}$ | $194^{+30}_{-25}$ | $50.1^{+15.0}_{-11.1}$ | $43.8^{+15.3}_{-10.8}$ | $19.6^{+10.6}_{-6.5}$ | $17.0^{+11.1}_{-6.2}$ | $9.53^{+7.30}_{-3.81}$ | $7.40^{+6.57}_{-3.18}$ | $5.16^{+5.20}_{-2.36}$ | $3.66^{+3.92}_{-1.72}$ | $2.35^{+2.86}_{-1.16}$ | $1.66^{+2.32}_{-0.87}$ |
| Nucl. | $^{130}$In | $^{129}$Cd | $^{128}$Ag | $^{127}$Pd | $^{126}$Rh | $^{125}$Ru | $^{124}$Tc | $^{123}$Mo | $^{122}$Nb | $^{121}$Zr | $^{120}$Y | $^{119}$Sr |
| Exp. | $290 \pm 20$ | $154 \pm 2$ | $58 \pm 5$ | $38 \pm 2$ | $19 \pm 3$ | | | | | | | |
| RQRPA | 519 | 183 | 90.8 | 51.4 | 31.6 | 20.6 | 14.0 | 9.73 | 6.91 | 5.05 | 3.65 | 2.67 |
| NPA | $340^{+53}_{-45}$ | $289^{+48}_{-40}$ | $59.0^{+12.7}_{-10.1}$ | $50.8^{+17.7}_{-12.5}$ | $23.7^{+9.4}_{-6.4}$ | $20.1^{+13.1}_{-7.4}$ | $10.5^{+6.5}_{-3.7}$ | $7.99^{+7.38}_{-3.50}$ | $4.76^{+4.10}_{-2.02}$ | $3.25^{+3.40}_{-1.51}$ | $2.44^{+2.57}_{-1.14}$ | $1.44^{+1.66}_{-0.70}$ |

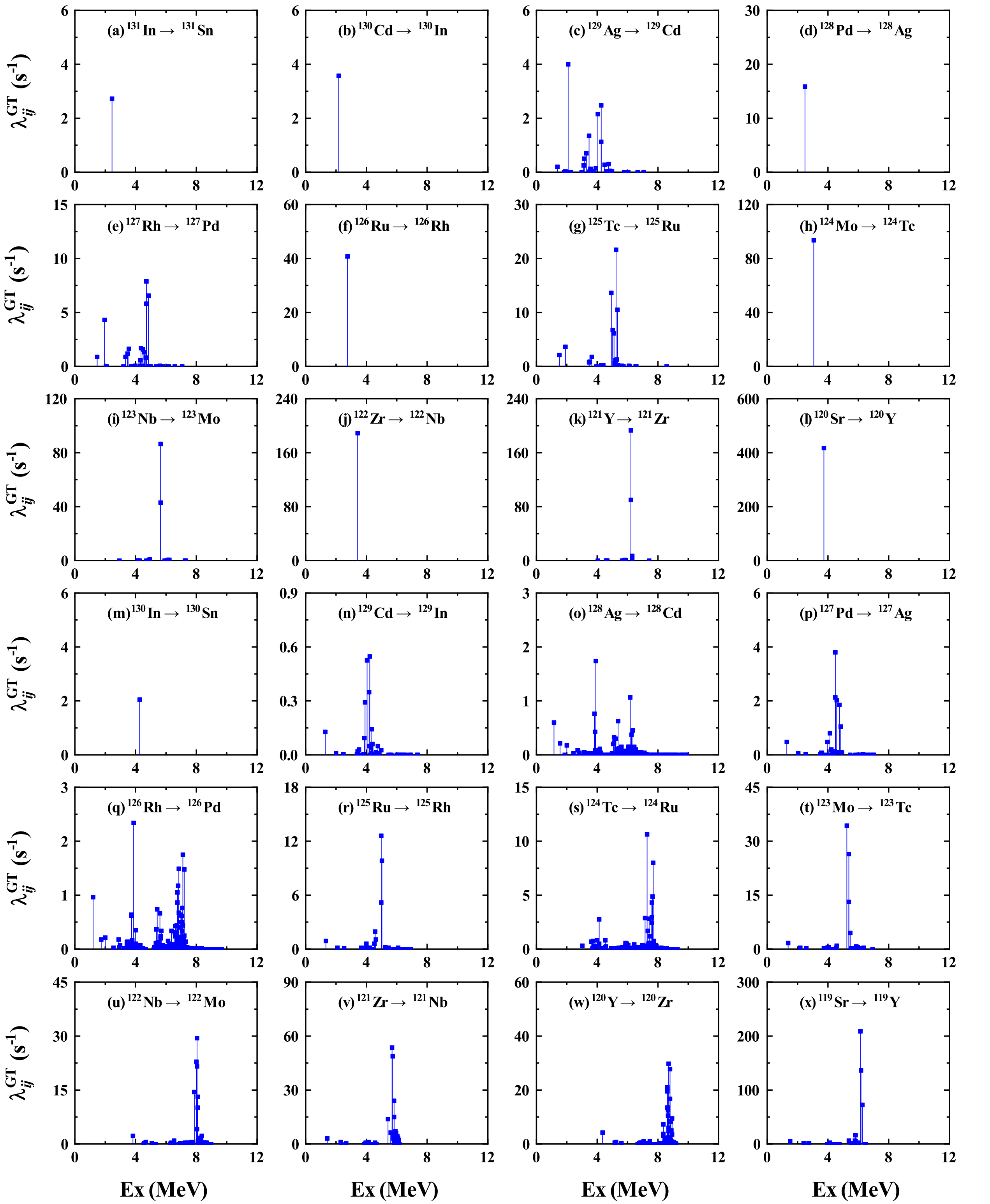


FIG. 6. Gamow-Teller decay rates of the parent ground state ($\lambda_{ij}^{\mathrm{GT}}$ with $j = 0$) versus excitation energy of populated states for daughter nuclei. (a)–(l) correspond to $N = 82$ isotones, and (m)–(x) correspond to $N = 81$ isotones. Proton number $38 \leqslant Z \leqslant 49$.

even-$Z$ neighbors by about 2 MeV. This regularity cancels out with the odd-even staggering of $Q_\beta$, and as a consequence, largely quenches the odd-even staggering of half-lives along the isotonic chains, as we have shown in Fig. 5.

From Fig. 3, we have seen that there are quasidegeneracies around the ground states of some $N = 82$ and 81 isotones with odd protons. Such quasidegeneracies might be of interest, because in the stellar environment excited states and ground states of atomic nuclei follows the Boltzmann distribution, and thus the low-lying isomers (the lowest $1/2^-$ state of $^{125}$Tc, the lowest $9/2^+$ state of $^{123}$Nb, and the lowest $11/2^-$ states of $N = 81$ odd mass isotones, see Fig. 3) also contribute to the nucleosynthesis process [77]. For this reason, in this paper we have calculated the half-lives of these low-lying states. Our results are as follows: 10.6 ms for the $\frac{1}{2}^-$ state of $^{125}$Tc, 5.00 ms for the $\frac{9}{2}^+$ state of $^{123}$Nb, and 296, 51.5, 20.3, 8.03, 3.26, 1.44 ms for the $\frac{11}{2}^-$ states of $^{129}$Cd, $^{127}$Pd, $^{125}$Ru, $^{123}$Mo, $^{121}$Zr, $^{119}$Sr, respectively. According to our calculation, the difference between resultant half-lives with such quasidegeneracies and those without the degeneracies are below 12%, and this difference is much smaller than uncertainties originated from nuclear masses. Namely, our calculations show that, for the $N = 81$ and 82 isotones, the quasidegeneracy of the two lowest states would not yield significant impacts on the $r$-process simulation. The results for odd-odd parent nuclei are similar. In Fig. 3 one sees that there are many states which are very close to the ground states of odd-odd parent nuclei. For the set of states with noncollective pairs constructed by the same unpaired proton hole and neutron hole, calculated half-lives are close to each other, while for those with noncollective pairs constructed by different unpaired proton hole and neutron hole, calculated half-lives are slightly different. However, changes of $\beta$-decay half-lives by considering those excited states are within within 10%. Therefore the quasidegeneracy close to the ground states for the odd-odd nuclei does not change the pattern of the $r$-process rates, as for the above case of odd-mass isotones with $N = 81$ and 82.

In this paper, we present our calculated results of the electromagnetic moments for ground states of odd mass nuclei. For the spin $g$ factors, we use the values $g_{s\pi} = 5.586 \times 0.7\ \mu_N$ and $g_{s\nu} = -3.826 \times 0.7\ \mu_N$ (0.7 is the usual quenching factor in the shell model calculations). The orbital $g$ factors are fixed as $g_{l\pi} = 1$ and $g_{l\nu} = 0$. As for the effective charges of valence nucleons, we follow the relation $|e_\nu| = \delta e$, $|e_\pi| = (1+\delta)e$ in Ref. [78] and fix them as $e_\nu = -0.5$, $e_\pi = -1.5$, *a priori*. The calculated electrical quadrupole moments ($\mathcal{Q}$) and magnetic moments ($\mu$) are shown in Tables III and IV. From the table one sees that most of electric quadrupole moments $\mathcal{Q}$ are in the magnitude of $10^{-1}\ e$b and those of magnetic moments are about several $\mu_N$.

### C. Robustness of calculated results

In this subsection we investigate the robustness of our calculated results. Our discussion of robustness focuses on the configuration space, two-body interactions, and the effective $g_A$ value.

In this paper we assume $S$-pair condensation for states of parent nuclei, which is expected to be a very good truncation scheme for the ground states of semimagic nuclei or isotones (isotopes) close to the magic number. To investigate whether or not other nucleon pairs play an essential role in this work, in addition to optimized $S$ pairs, we further consider collective $D$ pairs,

$$D_\eta^{(2)\dagger} = \sum_{j_\eta j'_\eta} y(j_\eta j'_\eta 2)\big(a^\dagger_{j_\eta} \times a^\dagger_{j'_\eta}\big)^{(2)} \tag{18}$$

with the structure coefficients $y(j_\eta j'_\eta 2)$ obtained by using the broken-pair approximation (BPA). We perform calculations in the $SD$-pair configuration space for the ground state wave functions of the even-even parent nuclei $^{130}$Cd, $^{128}$Pd, $^{126}$Ru, and $^{124}$Mo. All overlaps between the wave functions obtained in the $SD$-pair space and the $S$-pair condensation are larger than 0.997. This demonstrates that $S$-pair condensation adopted in this paper for parent nuclei are very good approximation, as expected.

A more relevant question is on the configuration space of excited states which are involved in given $\beta$-decay process, for daughter nuclei. For this purpose, we recalculate the half-lives with collective $SD$ configuration spaces for both parent and daughter nuclei. In Fig. 7 the partial decay rates of $^{128}$Pd,

TABLE III. Calculated electrical quadrupole moments $\mathcal{Q}$ (in $e$b) and magnetic moments $\mu$ (in $\mu_N$) of low-lying states of odd mass isotones with $N = 82$ and 80. $g$ factors $g_{l\pi} = 1\ \mu_N$, $g_{l\nu} = 0$, $g_{s\pi} = 5.586 \times 0.7\ \mu_N$, $g_{s_\nu} = -3.826 \times 0.7\ \mu_N$. Effective charges $e_\pi = -1.5\ e$, $e_\nu = -0.5\ e$.

| Level | $\mathcal{Q}_{\rm th}$ | $\mu_{\rm th}$ | $\mathcal{Q}_{\rm th}$ | $\mu_{\rm th}$ | $\mathcal{Q}_{\rm th}$ | $\mu_{\rm th}$ | $\mathcal{Q}_{\rm th}$ | $\mu_{\rm th}$ |
|---|---|---|---|---|---|---|---|---|
| | $^{131}$In | | $^{129}$In | | $^{129}$Ag | | $^{127}$Ag | |
| $\frac{9}{2}^+_1$ | 0.308 | 5.96 | 0.345 | 5.93 | 0.180 | 5.96 | 0.207 | 5.95 |
| $\frac{1}{2}^-_1$ | – | 0.02 | – | <0.01 | – | 0.02 | – | <0.01 |
| | $^{127}$Rh | | $^{125}$Rh | | $^{125}$Tc | | $^{123}$Tc | |
| $\frac{9}{2}^+_1$ | 0.060 | 5.96 | 0.076 | 5.95 | −0.050 | 5.96 | −0.046 | 5.95 |
| $\frac{1}{2}^-_1$ | – | 0.02 | – | <0.01 | – | 0.02 | – | 0.01 |
| | $^{123}$Nb | | $^{121}$Nb | | $^{121}$Y | | $^{119}$Y | |
| $\frac{9}{2}^+_1$ | −0.152 | 5.96 | −0.156 | 5.95 | −0.238 | 5.96 | −0.248 | 5.94 |
| $\frac{1}{2}^-_1$ | – | 0.02 | – | 0.01 | – | 0.02 | – | 0.02 |

TABLE IV. Same as Table III, but for isotones with $N = 81$. The experimental quadrupole moments compiled in the NNDC database are 0.02, −0.04 $e$b for the $\frac{11}{2}^-_1$ and $\frac{3}{2}^+_1$ states of $^{131}$Sn, and 0.57, 0.132 $e$b for the $\frac{11}{2}^-_1$ and $\frac{3}{2}^+_1$ states of $^{129}$Cd. The experimental magnetic moments are −1.28, 0.75 $\mu_N$ for the $\frac{11}{2}^-_1$ and $\frac{3}{2}^+_1$ states of $^{131}$Sn, and −0.71, 0.85 $\mu_N$ for the $\frac{11}{2}^-_1$ and $\frac{3}{2}^+_1$ states of $^{129}$Cd, which are reasonably consistent with our calculations.

| Level | $\mathcal{Q}_{\rm th}$ | $\mu_{\rm th}$ | $\mathcal{Q}_{\rm th}$ | $\mu_{\rm th}$ | $\mathcal{Q}_{\rm th}$ | $\mu_{\rm th}$ | $\mathcal{Q}_{\rm th}$ | $\mu_{\rm th}$ |
|---|---|---|---|---|---|---|---|---|
| | $^{131}$Sn | | $^{129}$Cd | | $^{127}$Pd | | $^{125}$Ru | |
| $\frac{11}{2}^-_1$ | 0.128 | −1.34 | 0.210 | −1.33 | 0.251 | −1.32 | 0.269 | −1.32 |
| $\frac{1}{2}^+_1$ | – | −1.34 | – | −1.31 | – | −1.29 | – | −1.28 |
| $\frac{3}{2}^+_1$ | 0.057 | 0.80 | 0.087 | 0.83 | 0.107 | 0.84 | 0.119 | 0.85 |
| | $^{123}$Mo | | $^{121}$Zr | | $^{119}$Sr | | | |
| $\frac{11}{2}^-_1$ | 0.270 | −1.32 | 0.260 | −1.32 | 0.124 | −1.34 | | |
| $\frac{1}{2}^+_1$ | – | −1.27 | – | −1.28 | – | −1.34 | | |
| $\frac{3}{2}^+_1$ | 0.124 | 0.85 | 0.121 | 0.84 | 0.055 | 0.80 | | |

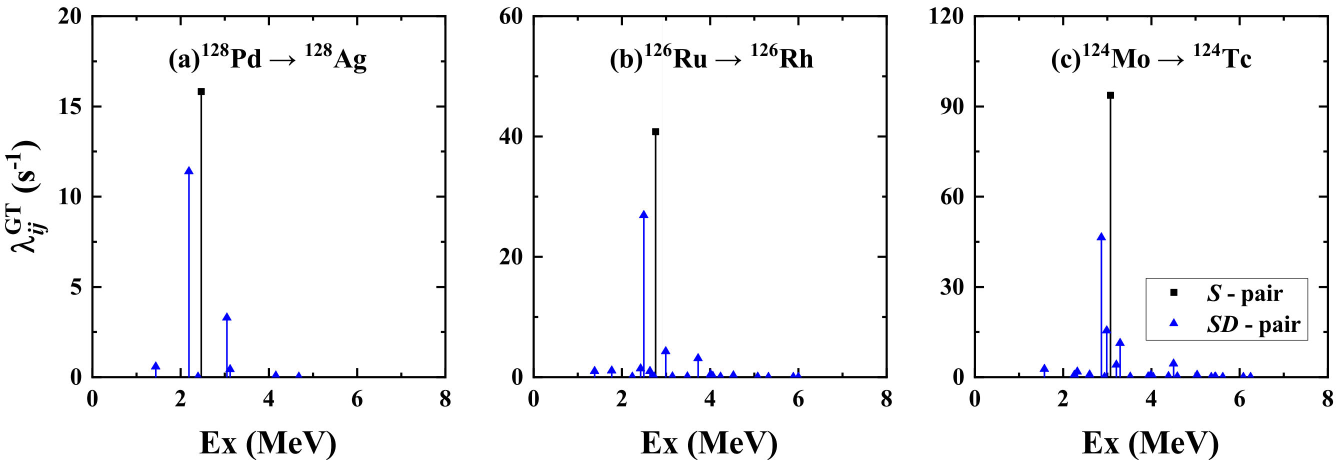


FIG. 7. Gamow-Teller decay rates from the ground state of $^{128}$Pd, $^{126}$Ru, and $^{124}$Mo in the *SD*-pair (triangles in blue) and *S*-pair (solid squares in black) truncated spaces, versus excitation energies of daughter nuclei, populated by the GT transitions.

$^{126}$Ru and $^{124}$Mo in the extended configuration spaces are plotted by using solid triangles in blue. The result obtained by assuming *S*-pair condensation is also plotted by using solid square in black, for comparison [same as in Fig. 6(d), 6(f), 6(h)]. One sees that there are a number of fragmentations in the *SD*-pair approximation, yet the integral of transition rates remain to be almost unchanged. For the three nuclei in Fig. 7, $^{128}$Pd, $^{126}$Ru, and $^{124}$Mo, the calculated half-lives are 43.8 ms, 17.0 ms, and 7.40 ms in the *S*-pair truncation, and are 43.9 ms, 17.2 ms, and 7.70 ms in the *SD*-pair truncation, respectively. The situation is similar for other nuclei studied in this paper.

Next we investigate the robustness of our calculated $\beta$ decay strengths with variation of the residual two-body interactions. Towards this goal, we introduce a few adjustable factors in our Hamiltonian defined in Eq. (5):

$$H = H_0 + x_P H_P + x_Q H_{QQ} + x_{\rm GT} H_{\rm GT} \ , \qquad (19)$$

where $x_P$, $x_Q$, and $x_{\rm GT}$ are multipliers on corresponding parameters in Table I. Let us take the $\beta$ decay $^{126}$Ru $\rightarrow$ $^{126}$Rh + $e^- + \bar{\nu}_e$ as an example. We calculate its half-life corresponding to individual changes of multipliers $x_P$, $x_Q$, and $x_{\rm GT}$, within a range of 0–2. The results are plotted in Fig. 8. From this figure, one sees that the half-life increases with $x_P$ and $x_{\rm GT}$ slowly, and is not sensitive to $x_Q$. We note that although $x_P$ and $x_{\rm GT}$ have similar effects on calculated half-life, their mechanisms are different—the increase of $x_P$ strengths enhances the level mixing in the ground state, and the increase of $x_{\rm GT}$ yields larger excitation energy of the $1^+$ state. For the sake of comparison, we also calculate the half-life as a function of $Q_\beta$, and plot the result in Fig. 8, the scale above are the evaluated uncertainty of $Q_\beta$ in the BML mass model. Clearly, the increase of $Q_\beta$ enhances the phase contribution of the leptons, and consequently reduces the half-life. As is well known, the calculated half-life is very sensitive to $Q_\beta$ (shown by the red dash-dot-dot line), i.e., the uncertainty of about 2 MeV in $Q_\beta$ of the $^{126}$Ru leads to a change in the calculated $\beta$-decay half-life by a factor of 2.

Finally we come to the uncertainty related to the parametrization of $g_A$. In this paper we fix the value of $g_A$ by using experimental results of $\beta$-decay half-lives for specific states of $^{131}$In and $^{130}$In, as explained at the end of Sec. III A. It is interesting to investigate the uncertainty of our calculated results involving of our $g_A$ values, and this could be done by optimizing $g_A$ with another set of experimental data. Towards this goal, we perform $\chi^2$ fitting of the logarithmic half-lives for all accessible experimental data, individually for $N = 81$ and 82 isotones. The resultant $g_A^2$ is 0.416 for $N = 82$, and 0.535 for $N = 81$ isotones, which would yield systematically our calculated $\beta$-decay rates larger than those presented in this paper, by 8% for $N = 82$ and 30% for $N = 81$, respectively. We note that this uncertainty is smaller by far than those originated from the uncertainty of the nuclear mass prediction, as discussed above and shown in Fig. 8.

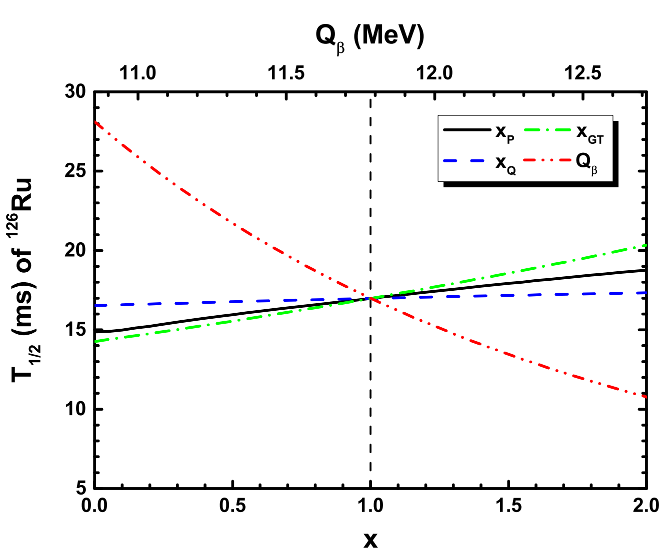


FIG. 8. Half-life of $^{126}$Ru versus multipliers on the interaction parameters and the $\beta$-decay energy. $x_P$, $x_{QQ}$, and $x_{\rm GT}$ are multipliers of the $H_P$, $H_{QQ}$, and $H_{\rm GT}$ terms, respectively, in Eq. (4). The range of $Q_\beta$ is adopted to be the theoretical uncertainty in the BML mass model.

## IV. SUMMARY AND PROSPECTIVE

In this article we have applied the nucleon-pair approximation (NPA) in the calculation of $\beta$-decay half-lives of $N = 81$ and 82 isotones with proton number $Z$ ranging from 39 to 49. The Hamiltonian we used is a phenomenological pairing plus quadrupole interaction extended by the Gamow-Teller force. The parameters in the Hamiltonian are fixed by reproducing experimental energy spectra of $^{130}$Sn, $^{130}$In, and $^{130}$Cd.

A main feature of our calculations is that we assume $S$ pair condensation in the ground state of parent nuclei. The validity of this truncation is exemplified by further considering collective $D$ nucleon pairs. Our calculated half-lives are well consistent with accessible experimental data and some other theoretical evaluations in Refs. [21,23,26]. We have demonstrated that the calculated $\beta$-decay half-life is very sensitive to the $\beta$-decay energy. As an example, an uncertainty of about 2 MeV in the $\beta$-decay energy of $^{126}$Ru would lead to difference of a factor of 2 in the calculated half-life, which is much more significant than the uncertainty originated from the parametrization in the NPA calculations. Therefore accurate measurements and reliable predictions on nuclear masses are crucial not only for the calculation of neutron capture rates [6], but also for the simulation of weak decay process.

Although this work is restricted in the region of $A \approx 130$, the fundamental idea of the NPA is applicable to the waiting-point $N = 126$ isotones, for which the contribution of first-forbidden (FF) transitions plays an significant role in the estimation of half-lives [26]. Therefore one of the next steps is to develop the calculation of the FF transition matrix elements in the NPA framework.

## ACKNOWLEDGMENTS

We are grateful to Professors H. Jin, Q. J. Zhi, and L. J. Wang for discussions. We also thank the National Natural Science Foundation of China (Grants No. 11975151 and 11961141003) and the MOE Key Lab for Particle Physics, Astrophysics and Cosmology for financial support.

## APPENDIX: TECHNICAL DETAILS OF CALCULATION OF REDUCED GT MATRIX ELEMENT

In this Appendix, we present our calculation formulas of the reduced GT matrix element. The GT operators of $\beta^+$ and $\beta^-$ decays are written as

$$\sigma\tau_+ = \sum_{j_\nu j_\pi} q_1(j_\nu j_\pi)\left(a^\dagger_{j_\nu} \times \tilde{a}_{j_\pi}\right)^{(1)} ,$$
$$\sigma\tau_- = \sum_{j_\pi j_\nu} q_1(j_\pi j_\nu)\left(a^\dagger_{j_\pi} \times \tilde{a}_{j_\nu}\right)^{(1)} , \tag{A1}$$

where $j_\pi$ and $j_\nu$ represent the proton and neutron levels, respectively. The structure coefficients, $q_1$ in Eq. (10), follow that

$$q_1(j_\pi j_\nu) = (-)^{j_\pi + j_\nu + 1} q_1(j_\nu j_\pi). \tag{A2}$$

In the NPA framework the model space is constructed simply by coupling neutron basis states and proton basis states,

$$|\alpha_\nu J_\nu \alpha_\pi J_\pi ; J\rangle = \left(A^{J_\nu\dagger}_{\alpha_\nu} \times A^{J_\pi\dagger}_{\alpha_\pi}\right)^{(J)}|0\rangle , \tag{A3}$$

where $J_\nu$ and $J_\pi$ represent the angular momenta of the neutron and proton bases, and $\alpha_\nu$, $\alpha_\pi$ are the additional quantum numbers. The reduced GT matrix element is as follows:

$$\begin{aligned}&\langle \alpha'_\nu J'_\nu \alpha'_\pi J'_\pi , J' || \sigma\tau_- || \alpha_\nu J_\nu \alpha_\pi J_\pi , J\rangle \\ &= (-)^{n_\nu} \sum_{j_\nu j_\pi} q_1(j_\nu j_\pi) \begin{bmatrix} J_\nu & J_\pi & J \\ j_\nu & j_\pi & 1 \\ J'_\nu & J'_\pi & J' \end{bmatrix} \\ &\times \langle \alpha'_\nu J'_\nu \| a^\dagger_{j_\nu} \| \alpha_\nu J_\nu\rangle \langle \alpha'_\pi J'_\pi \| \tilde{a}_{j_\pi} \| \alpha_\pi J_\pi\rangle .\end{aligned} \tag{A4}$$

Note that the reduced matrix element of an annihilation operator is directly related to its creation operator,

$$\langle \alpha' J' || \tilde{a}_j || \alpha J\rangle = (-)^{J+j-J'} \sqrt{\frac{2J+1}{2J'+1}} \langle \alpha J || a^\dagger_j || \alpha' J'\rangle . \tag{A5}$$

The basis of like nucleons is constructed by successively coupling nucleon pairs,

$$\begin{aligned}|\alpha J_N M_N\rangle &= |j r_1 r_2 \ldots r_N , J_1 J_2 \ldots J_N M_N\rangle \\ &= \{\cdots [(A^{j\dagger} \times A^{r_1\dagger})^{(J_1)} \times A^{r_2\dagger}]^{(J_2)} \\ &\quad \times \cdots \times A^{r_N\dagger}\}^{(J_N)}_{M_N} |0\rangle\end{aligned} \tag{A6}$$

with $A^{j\dagger} = a^\dagger_j$ for an odd-nucleon system and $A^{j\dagger} = 1$ for an even-nucleon system. A reduced matrix element of the single-particle creation operator between such bases is calculated by

$$\begin{aligned}&\langle j' r'_1 \ldots r'_N , J'_1 \ldots J'_N || a^\dagger_{j''} || j r_1 \ldots r_N , J_1 \ldots J_N\rangle \\ &= - \sum_{L_1 \ldots L_{N+1}} Q_N(j'') Q_{N-1}(j'') \ldots Q_1(j'') \\ &\times \langle j' r'_1 \ldots r'_N , J'_1 \ldots J'_N | L_1 r_1 \ldots r_N , L_2 \ldots L_{N+1}\rangle ,\end{aligned} \tag{A7}$$

where $L_1$ represents the angular momentum of a noncollective pair $(a^\dagger_j \times a^\dagger_{j''})^{L_1}$, and $L_i (i \neq 1)$ run over all possible coupling angular momenta among the nucleon pairs. $Q_i(j'')$ is the propagator to cross $a^\dagger_{j''}$ over the $i$th pair,

$$Q_i(j'') = (-)^{J_{i-1} + L_{i+1} - J_i - L_i} U(r_i L_{i+1} J_{i-1} j'' ; L_i J_i) .$$

Here, $U(r_i L_{i+1} J_{i-1} j''; L_i J_i)$ is the Racha coefficient. The overlap matrix element on the right-hand side of Eq. (A7) was given in Ref. [30].

[1] E. M. Burbidge, G. R. Burbidge, W. A. Fowler, and F. Hoyle, Rev. Mod. Phys. **29**, 547 (1957).

[2] J. J. Cowan, F.-K. Thielemann, and J. W. Truran, Phys. Rep. **208**, 267 (1991).

[3] K.-L. Kratz, J. Bitouzet, F.-K. Thielemann, P. Moller, and B. Pfeiffer, Astrophys. J. **403**, 216 (1993).

[4] F.-K. Thielemann, M. Eichler, I. V. Panov, and B. Wehmeyer, Annu. Rev. Nucl. Part. Sci. **67**, 253 (2017).

[5] M. R. Mumpower, R. Surman, D.-L. Fang, M. Beard, P. Möller, T. Kawano, and A. Aprahamian, Phys. Rev. C **92**, 035807 (2015).

[6] C. Ma, Z. Li, Z. M. Niu, and H. Z. Liang, Phys. Rev. C **100**, 024330 (2019).

[7] K.-L. Kratz, F. K. Thielemann, W. Hillebrandt, P. Möller, V. Härms, A. Wöhr, and J. W. Truran, J. Phys. G **14**, S331 (1988).

[8] P. O. Strom, D. L. Love, A. E. Greendale, A. A. Delucchi, D. Sam, and N. E. Ballou, Phys. Rev. **144**, 984 (1966).

[9] H. Huck, M. L. Pérez, J. J. Rossi, and H. M. Sofía, Phys. Rev. C **24**, 2227 (1981).

[10] K.-L. Kratz, B. Pfeiffer, F.-K. Thielemann, and W. B. Walters, Hype. Inte. **129**, 185 (2000).

[11] M. Hannawald, V. N. Fedoseyev, U. Köster, K.-L. Kratz, V. I. Mishin, W. F. Mueller *et al.*, Nucl. Phys. A **688**, 578 (2001).

[12] B. Pfeiffer, K.-L. Kratz, F.-K. Thielemann, and W. B. Walters, Nucl. Phys. A **693**, 282 (2001).

[13] P. T. Hosmer, H. Schatz, A. Aprahamian, O. Arndt, R. R. C. Clement, A. Estrade *et al.*, Phys. Rev. Lett. **94**, 112501 (2005).

[14] G. Lorusso *et al.*, Phys. Rev. Lett. **114**, 192501 (2015).

[15] P. Möller, J. R. Nix, and K.-L. Kratz, At. Data Nucl. Data Tables **66**, 131 (1997).

[16] Z. M. Niu, H. Z. Liang, B. H. Sun, W. H. Long, and Y. F. Niu, Phys. Rev. C **99**, 064307 (2019).

[17] J. Engel, M. Bender, J. Dobaczewski, W. Nazarewicz, and R. Surman, Phys. Rev. C **60**, 014302 (1999).

[18] I. N. Borzov, S. Goriely, and J. M. Pearson, Nucl. Phys. A **621**, 307 (1997).

[19] I. N. Borzov and S. Goriely, Phys. Rev. C **62**, 035501 (2000).

[20] P. Möller, B. Pfeiffer, and K.-L. Kratz, Phys. Rev. C **67**, 055802 (2003).

[21] D.-L. Fang, B. A. Brown, and T. Suzuki, Phys. Rev. C **88**, 034304 (2013).

[22] Z. M. Niu, Y. F. Niu, H. Z. Liang, W. H. Long, T. Nikšić, D. Vretenar, and J. Meng, Phys. Lett. B **723**, 172 (2013).

[23] T. Marketin, L. Huther, and G. Martnez-Pinedo, Phys. Rev. C **93**, 025805 (2016).

[24] J. J. Cuenca-Garcıa, G. Martinez-Pinedo, K. Langanke, F. Nowacki, and I. N. Borzov, Eur. Phys. J. A **34**, 99 (2007).

[25] T. Suzuki, T. Yoshida, T. Kajino, and T. Otsuka, Phys. Rev. C **85**, 015802 (2012).

[26] Q. Zhi, E. Caurier, J. J. Cuenca-Garcia, K. Langanke, G. Martinez-Pinedo, and K. Sieja, Phys. Rev. C **87**, 025803 (2013).

[27] Z.-C. Gao, Y. Sun, and Y.-S. Chen, Phys. Rev. C **74**, 054303 (2006).

[28] L.-J. Wang, Y. Sun, and S. K. Ghorui, Phys. Rev. C **97**, 044302 (2018).

[29] J.-Q. Chen, B.-Q. Chen, and A. Klein, Nucl. Phys. A **554**, 61 (1993); J. Q. Chen, *ibid.* **562**, 218 (1993); **626**, 686 (1997).

[30] Y. M. Zhao, N. Yoshinaga, S. Yamaji, J. Q. Chen, and A. Arima, Phys. Rev. C **62**, 014304 (2000).

[31] Y. M. Zhao, S. Yamaji, N. Yoshinaga, and A. Arima, Phys. Rev. C **62**, 014315 (2000).

[32] L. Y. Jia, H. Zhang, and Y. M. Zhao, Phys. Rev. C **75**, 034307 (2007).

[33] L. Y. Jia, H. Zhang, and Y. M. Zhao, Phys. Rev. C **76**, 054305 (2007).

[34] Y. Lei, Z. Y. Xu, Y. M. Zhao, and A. Arima, Phys. Rev. C **82**, 034303 (2010).

[35] H. Jiang, G. J. Fu, Y. M. Zhao, and A. Arima, Phys. Rev. C **84**, 034302 (2011).

[36] K. Higashiyama and N. Yoshinaga, Phys. Rev. C **83**, 034321 (2011).

[37] M. Bao, H. Jiang, Y. M. Zhao, and A. Arima, Phys. Rev. C **101**, 014316 (2020).

[38] Y. Bao, Y. Y. Cheng, and X.-R. Zhou, Phys. Rev. C **104**, 034312 (2021).

[39] B. C. He, H. T. Xue, L. Li, Y. A. Luo, Y. Zhang, F. Pan, and J. P. Draayer, Phys. Rev. C **101**, 014324 (2020).

[40] Y. A. Luo, Y. Zhang, X. F. Meng, F. Pan, and J. P. Draayer, Phys. Rev. C **80**, 014311 (2009).

[41] B. C. He, S. Y. Zhang, L. Li, Y. A. Luo, Y. Zhang, F. Pan, and J. P. Draayer, Phys. Rev. C **105**, 044332 (2022).

[42] G. J. Fu, Y. Lei, Y. M. Zhao, S. Pittel, and A. Arima, Phys. Rev. C **87**, 044310 (2013).

[43] G. J. Fu, J. J. Shen, Y. M. Zhao, and A. Arima, Phys. Rev. C **87**, 044312 (2013).

[44] G. J. Fu, Y. Y. Cheng, Y. M. Zhao, and A. Arima, Phys. Rev. C **94**, 024336 (2016).

[45] Y. Y. Cheng, Y. M. Zhao, and A. Arima, Phys. Rev. C **97**, 024303 (2018).

[46] Y. M. Zhao and A. Arima, Phys. Rep. **545**, 1 (2014), and references therein.

[47] H. T. Xue, X. R. Zhou, S. Y. Zhang, B. C. He, Y. A. Luo, L. Li, F. Pan, and J. P. Draayer, Phys. Rev. C **105**, 014304 (2022).

[48] E. Fermi, Z. Phys. **88**, 161 (1934).

[49] M. E. Rose, *Relativistic Electron Theory* (John Wiley and Sons, New York, 1961).

[50] C. P. Bhalla and M. E. Rose, Phys. Rev. **128**, 774 (1962).

[51] Y. M. Zhao, N. Yoshinaga, S. Yamaji, and A. Arima, Phys. Rev. C **62**, 014316 (2000).

[52] V. A. Kuz-Min and V. G. Soloviev, Nucl. Phys. A **486**, 118 (1988).

[53] H. Homma, E. Bender, M. Hirsch, K. Muto, H. V. Klapdor-Kleingrothaus, and T. Oda, Phys. Rev. C **54**, 2972 (1996).

[54] J. Suhonen and O. Civitarese, Phys. Rep. **300**, 123 (1998).

[55] P. Sarriguren, Phys. Rev. C **87**, 045801 (2013).

[56] R. D. Lawson, *Theory of the Nuclear Shell Model* (Clarendon Press, Oxford, 1980), p. 7.

[57] I. Talmi, *Simple Models of Complex Nuclei: The Shell Model and Interacting Boson Model* (Harwood Academic Publishers, Chur, Switzerland, 1993), Vol. 23.

[58] K. Levenberg, Quart. Appl. Math. **2**, 164 (1944).

[59] D. W. Marquardt, J. Soc. Indust. Appl. Math. **11**, 431 (1963).

[60] Y. Khazov, I. Mitropolsky, and A. Rodionov, Nucl. Data Sheets **107**, 2715 (2006).

[61] B. Fogelberg, H. Gausemel, K. A. Mezilev, P. Hoff, H. Mach, M. Sanchez-Vega *et al.*, Phys. Rev. C **70**, 034312 (2004).

[62] A. Kankainen, J. Hakala, T. Eronen, D. Gorelov, A. Jokinen, V. S. Kolhinen *et al.*, Phys. Rev. C **87**, 024307 (2013).

[63] J. Taprogge, A. Jungclaus, H. Grawe, S. Nishimura, P. Doornenbal, G. Lorusso *et al.*, Phys. Rev. Lett. **112**, 132501 (2014).

[64] B. Singh, Nucl. Data Sheets **93**, 33 (2001).

[65] M. Hasegawa and K. Kaneko, Phys. Rev. C **59**, 1449 (1999).

[66] M. Hasegawa, K. Kaneko, and S. Tazaki, Nucl. Phys. A **674**, 411 (2000).
[67] M. Hasegawa, K. Kaneko, and S. Tazaki, Nucl. Phys. A **688**, 765 (2001).
[68] K. Kaneko, M. Hasegawa, and T. Mizusaki, Phys. Rev. C **66**, 051306(R) (2002).
[69] M. Hasegawa, K. Kaneko, and T. Mizusaki, Phys. Rev. C **71**, 044301 (2005).
[70] M. Wang, W. J. Huang, F. G. Kondev, G. Audi, and S. Naimi, Chin. Phys. C **45**, 030003 (2021).
[71] Z. M. Niu and H. Z. Liang, Phys. Rev. C **106**, L021303 (2022).
[72] P. Möller, W. D. Myers, H. Sagawa, and S. Yoshida, Phys. Rev. Lett. **108**, 052501 (2012).
[73] H. Jiang, G. J. Fu, B. Sun *et al.*, Phys. Rev. C **85**, 054303 (2012).
[74] N. Wang, M. Liu, X. Z. Wu, and J. Meng, Phys. Lett. B **734**, 215 (2014).
[75] J. T. Suhonen, Front. Phys. **5**, 55 (2017).
[76] T. Otsuka, T. Suzuki, R. Fujimoto, H. Grawe, and Y. Akaishi, Phys. Rev. Lett. **95**, 232502 (2005).
[77] A. Cameron, Astrophys. J. **130**, 452 (1959).
[78] A. Bohr and B. Mottelson, *Nuclear Structure* (Benjamin, New York, 1975), Vol. 1.